ChemComm

COMMUNICATION

Cite this: *Chem. Commun.*, 2019, **55**, 1899

Received 20th November 2018, Accepted 9th January 2019

DOI: 10.1039/c8cc09220f

rsc.li/chemcomm

Thermally activated delayed fluorescence and room-temperature phosphorescence in naphthyl appended carbazole–quinoline conjugates, and their mechanical regulation†

Indranil Bhattacharjee, Nirmalya Acharya and Debdas Ray *

The influences of naphthyl and/or phenyl rings at the 2,4-positions of the quinolinyl fragments in carbazole–quinoline conjugates are studied. The centric phase of one of the conjugates (β-CQNN) revealed both thermally activated delayed fluorescence (TADF) and room-temperature phosphorescence (RTP), while prompt fluorescence and RTP were observed in the non-centric phase (α-CQNN) that can regenerate the emission features of β-CQNN *via* mechanical grinding. This unique observation is explained by the modulation of the higher-lying triplet (T_2) energy level caused by conformational change.

Research on thermally activated delayed fluorescence (TADF)[1] and room-temperature phosphorescence (RTP)[2] in purely organic molecules has showcased exciting and unique capabilities of efficient light-emission, creating myriad opportunities for applications. TADF *via* reverse intersystem crossing (rISC) from the excited lowest triplet (T_1) to singlet (S_1) state shed light on the development of organic light-emitting diodes (OLEDs) because 100% internal quantum efficiency can be achieved by harvesting both singlet and triplet excitons. In addition, to observe RTP *via* harvesting of triplet excitons, economically cheaper purely organic materials appear to be of great interest for applications of display devices,[3] sensors,[4] advanced security imaging,[5] and bio-imaging[6] due to the utilization of their triplet energy and long lifetimes. Most of the reported organic systems[1] have shown that a low energy gap between the S_1 and T_1 ($\Delta E_{S_1-T_1}$) states is required to observe TADF, while the rigidity of the molecular backbone, air-proof matrices, and optimized triplet energy levels play important roles in controlling non-radiative pathways to observe RTP.[3–6] Taken together, achieving both TADF *via* rISC from the higher-lying triplet (T_n, $n > 1$) to S_1 state and RTP from the T_1 state has become a difficult task in photophysics due to the difficulty in tuning the excited energy levels of a single molecule (Fig. 1).

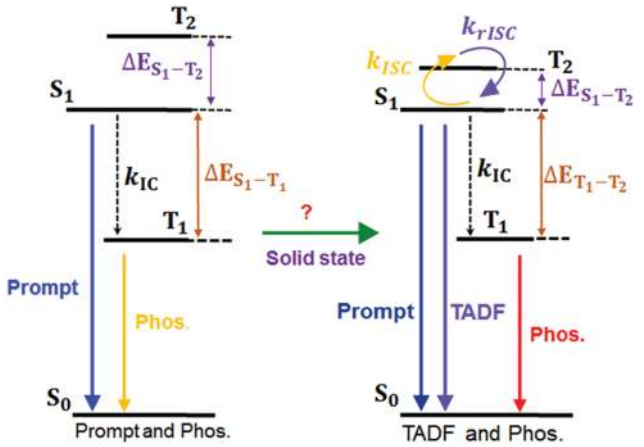

Fig. 1 Jablonski diagram of mechano-switching dual emission.

On the other hand, organic mechanoluminescent materials (OMLMs), whose photophysical properties change upon exposure to a pre-defined external stimulus in a highly selective and predictable manner, have attracted increasing attention in the fields of sensors,[7] memory chips,[8] and security inks.[9] Mechanoluminescence (ML) behaviour in purely organic compounds can be achieved by either chemical structural change[10] that involves bond breaking or forming at the molecular level, or controlling the mode of molecular packing (physical structural change).[11,12] As is well known, the emission efficiency of organic materials often becomes very weak in the solid state due to the aggregation-caused quenching (ACQ) effect derived from the strong π–π stacking; thus the ML phenomenon becomes a challenging feat. Unfortunately, only a handful of molecular systems[13,14] have shown that mechanical force (MF) can alter their triplet energy levels *via* perturbation of intra- and inter-molecular interactions in the crystals, and thus can lead to changes in their optical properties in a controlled manner. However, studies of OMLMs that undergo conformational change upon exposure to MF remain limited because a common method for synthesis of such OMLMs is ill-understood. Therefore, it is imperative to design new ''smart'' OMLMs which would address

Department of Chemistry, Shiv Nadar University, NH-91, Tehsil Dadri, District Gautam Buddha Nagar, Uttar Pradesh, 201314, India. E-mail: debdas.ray@snu.edu.in

† Electronic supplementary information (ESI) available. CCDC 1872167, 1872168, 1878663 and 1878664. For ESI and crystallographic data in CIF or other electronic format see DOI: 10.1039/c8cc09220f

these limitations, and create new opportunities in ML applications. Previously, we have shown with a carbazole–quinoline conjugate[15] that both TADF *via* rISC from T_2 to S_1 and RTP from T_1 can be achieved due to the low energy gap between S_1 and T_2 ($\Delta E_{S_1-T_2}$) and the close proximity of T_2 and T_1 ($\Delta E_{T_1-T_2}$). We now demonstrate that such dual emission can also be realized with a naphthyl appended carbazole–quinoline conjugate (β-**CQNN**), which can be regenerated by mechanical grinding of α-**CQNN** that shows prompt fluorescence and RTP under ambient conditions. Single crystal X-ray diffraction (SCXRD) analysis of both α-**CQNN** (non-centric, $Pna2_1$) and β-**CQNN** (centric, $P2_1/n$) allowed us to directly and locally visualize the MFICC *via* rotation of the naphthyl and carbazolyl rings around the C–C and C–N single bonds. Detailed photophysical studies revealed that α-**CQNN** shows prompt fluorescence and RTP components, while both TADF *via* rISC from T_2 to S_1 and RTP features due to the radiative decay of the T_1 state were observed in β-**CQNN**. Theoretical calculations at the BLYP[16,17]/6-31g(d) level of theory in β-**CQNN** show low $\Delta E_{S_1-T_2}$ (0.016 eV) that may lead to TADF through rISC from the T_2 to S_1 state. The moderate values of $\Delta E_{T_1-T_2}$ (0.925 eV) and $\Delta E_{S_1-T_1}$ (0.941 eV) support the observation of RTP features from the T_1 to ground (S_0) state. On the other hand, a relatively high value of $\Delta E_{S_1-T_2}$ (0.732 eV) negates the possibility of TADF, while large values of $\Delta E_{S_1-T_1}$ (0.938 eV) and $\Delta E_{T_1-T_2}$ (1.673 eV) result in prompt fluorescence and RTP in α-**CQNN**. We anticipate that transduction of mechanical force into the conformational change can serve as a general strategy for the development of new OMLMs with desirable optical properties.

The target compounds **CQNN**, **CQNP**, and **CQPN** (Fig. 2) were prepared by simple multicomponent condensation reaction considering its modular and inexpensive nature. All the conjugates were characterized by NMR spectroscopy, high-resolution mass spectrometry, and X-ray analysis (ESI†).

Slow evaporation of toluene solutions of **CQNN** yielded rectangular shaped yellow crystals (α-**CQNN**), while rod shaped pale yellow crystals (β-**CQNN**) were obtained from a dichloromethane/hexane (2 : 1, v/v) solution mixture. Single crystal X-ray diffraction (SCXRD) analysis revealed that α-**CQNN** and β-**CQNN** were crystalized into non-centrosymmetric (orthorhombic, $Pna2_1$) and centrosymmetric (monoclinic, $P2_1/n$) phases (Table S1, ESI†). In α-**CQNN**, we observed that the carbazolyl and naphthyl rings attached at the C8, C2 and C4 positions of the quinolinyl fragment were significantly deviated from planarity. The corresponding torsions were measured to be −68.53°, 48.99° and 126.27°, when viewed along the C11–N2–C8–C9, C18–C17–C2–N1 and C28–C27–C4–C3 atoms, respectively (Fig. 3a and Fig. S6, Table S2, ESI†). Interestingly, torsions, which were found to be 80.06°, −133.07° and 88.99°, respectively, when viewed along the same atoms in β-**CQNN**, suggest a conformational change that occurred *via* rotation of the substituents around the C11–N2, C4–C27, and C2–C17 single bonds (Fig. 3b and Table S2, ESI†).

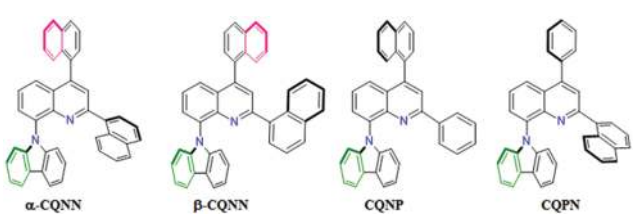

Fig. 2 Structures of α-**CQNN**, β-**CQNN**, **CQNP** and **CQPN**.

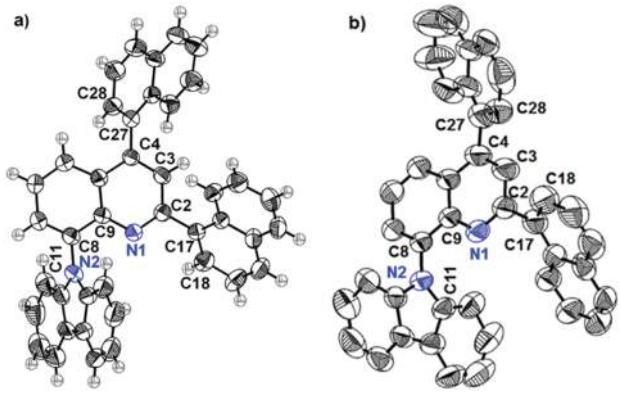

Fig. 3 Oak ridge thermal ellipsoid plots (50% probability ellipsoids) of (a) α-**CQNN** and (b) β-**CQNN**. The protons are omitted for clarity.

UV-vis (visible) studies of **CQNN** in toluene (1×10^{-5} M) solutions show structural absorption bands at 260, 282, 310, 330, 362, and 390 nm (Fig. S7a and Table S3, ESI†), which remain almost the same when other solvents are used (Fig. S7a, ESI†). In the steady state emission measurement of **CQNN** in toluene, we observed a single emission band (455 nm) (photoluminescence quantum yield, PLQY = 87.7%). With increasing solvent polarity a bathochromic shift of the λ_{450} was measured (Fig. S7b and Table S3, ESI†), indicating that **CQNN** is less polar in the Franck–Condon region (*i.e.*, the final potential energy surface accessed by the vertical transition from the ground vibrational state of the ground electronic state) than that of minima from which emission occurs.[1] Lifetime analysis using the time correlated single photon counting (TCSPC) technique shows a significant increase in the lifetime from 9.3 ns to 13.7 ns with increasing solvent polarity (Fig. S7c and Table S3, ESI†), which further substantiates the charge transfer (CT) character of the emission bands.

The photophysical properties of both crystals were systematically measured. The steady state emission spectrum of α-**CQNN** shows a broad emission peak at 432 nm (Fig. 4a) (PLQY, 18.7%). TCSPC analysis of this emission band shows a lifetime of 9.38 ns (Fig. S8, ESI†), indicating a prompt emission. Phosphorescence measurements with a 100 μs delay revealed a lower energy emission band at 545 nm with a lifetime of 1.8 ms (Fig. 4a, inset). These observations clearly suggest that α-**CQNN** exhibits dual-state emission *via* radiative decay of both singlet and triplet states. Likewise, only one red-shifted emission band at 465 nm was recorded in the steady-state emission of β-**CQNN** (PLQY, 22.7%). The most exciting feature is the observation of dual emission bands at 465 and 540 nm when a 100 μs detector delay was used in the phosphorescence measurement (Fig. 4b). In order to gain further insight, decay transient measurements were performed. TCSPC analysis of the λ_{465} at RT showed a bi-exponential decay with lifetimes of 7.4 ns and 10.1 μs (Fig. 4b). To confirm the origin of the longer-lived component (10.1 μs), temperature-dependent lifetime measurements were performed. We observed a continuous increase of the lifetime

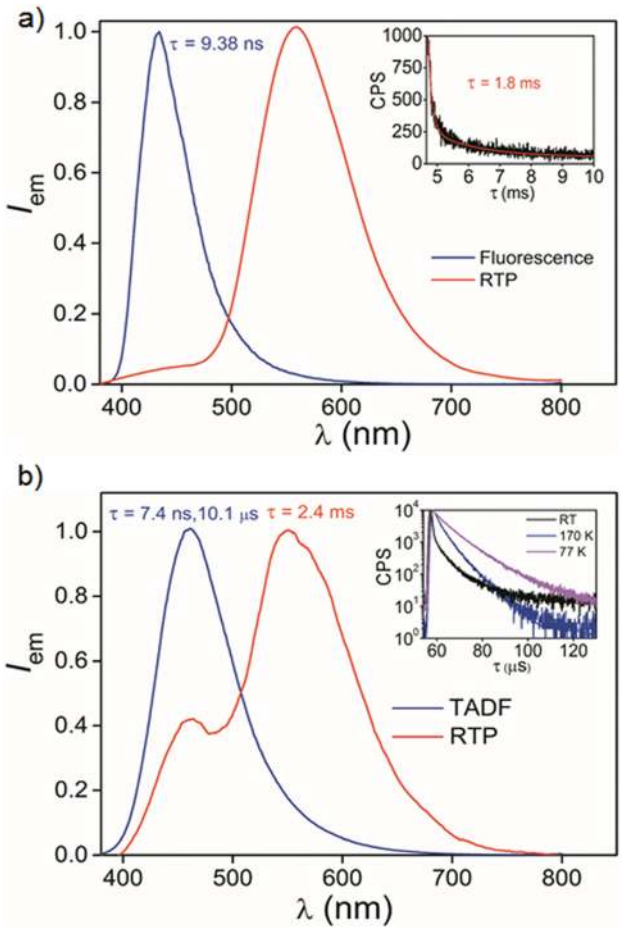

Fig. 4 PL features of (a) α-**CQNN** (crystals) and (b) β-**CQNN** (crystals). The inset shows phosphorescence decay kinetics at RT and from RT to 77 K.

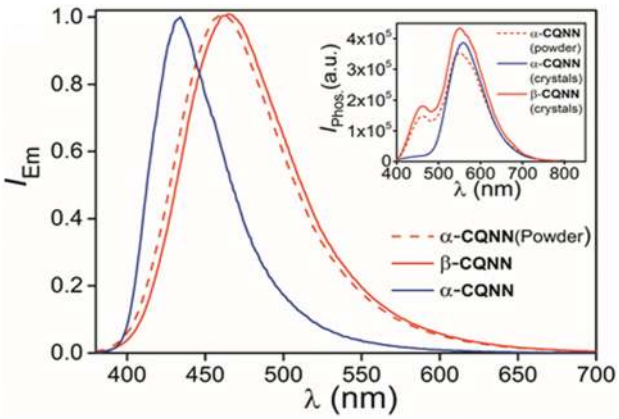

Fig. 5 Steady state PL features of α-**CQNN** (crystals), β-**CQNN** (crystals) and α-**CQNN** (powder). The inset shows RTP emissions.

from 10.1 μs (RT) to 82.1 μs (77 K) upon lowering the temperature (Fig. 4b). Furthermore, a monoexponential decay of the former band at 77 K was also observed. These observations suggest that the former band is TADF in nature. Since phosphorescence decay-transient measurements showed a longer-lifetime (2.4 ms) for the λ_{540}, we conclude that an additional low-energy triplet state also contributes to this emission. The calculated quantum yield values of phosphorescence (Φ_P), prompt fluorescence (Φ_{PF}), delayed fluorescence (Φ_{DF}), and intersystem crossing (Φ_{ISC}), and rate-parameters are also in line with the observation (Table S4, ESI†). Taken all together, we believe that β-**CQNN** shows light emission *via* TADF and RTP, while fluorescence and phosphorescence were observed in α-**CQNN**.

To test the effect of mechanical force, α-**CQNN** crystals were ground with a mortar and pestle. Surprisingly, a single emission peak at 461 nm, which closely overlapped with the steady state emission of β-**CQNN** (crystals), was recorded in the steady state measurement (Fig. 5). Phosphorescence measurements (100 μs detector delay) revealed two peaks at 461 and 538 nm (Fig. 5, inset). The observation of a bi-exponential (8.19 ns, 7.2 μs) feature at RT and a monoexponential feature at 77 K upon increasing the lifetime from 7.2 μs (RT) to 59 μs (77 K) unambiguously confirms the TADF character of the λ_{461} (Fig. S9, ESI†). In addition, the 2.1 ms lifetime of the latter band (538 nm) ensures the RTP feature. The thermodynamic rate parameters along with Φ_E were calculated (Table S5, ESI†). These results are in good agreement with the data obtained for β-**CQNN** (crystals). Furthermore, to gain knowledge of phase transition, powder X-ray diffraction (PXRD) and differential scanning calorimetric (DSC) measurements were performed. The PXRD pattern of α-**CQNN** (powder) closely overlaps with that of β-**CQNN** (crystals) (Fig. S10, ESI†), indicating a different phase which is crystalline in nature. Comparison of the PXRD data of α-**CQNN** (crystals) and α-**CQNN** (powder) with those of β-**CQNN** (crystals) (Fig. S10, ESI†) suggests that both α-**CQNN** (powder) and β-**CQNN** (crystals) belong to the same phase. DSC analysis of β-**CQNN** shows three distinct phase transitions, namely, $T_{\alpha-\beta}$ = ~66 °C, $T_{\beta-\gamma}$ = ~125 °C and $T_{\gamma-\delta}$ = ~150 °C, while only one phase transition (~112 °C) was observed for α-**CQNN** (Fig. S11, ESI†). After close inspection of PXRD, DSC and SCXRD analysis of both phases, we came to the conclusion that a MF induced conformational change (MFICC) has occurred, thus activating TADF and RTP *via* modulation of triplet energy levels.

To understand explicit evidence of the energy levels, we performed density functional theory (DFT) and time-dependent DFT (TD-DFT)[18] using the Gaussian 09[19] program. DFT and TDDFT studies at the BLYP/6-31G(d) level of theory reveal that two naphthyl and quinolinyl rings in α-**CQNN** contribute to S_1, T_1 and T_2 states (Fig. S12a, ESI†), while the major contributions of the quinolinyl ring and its naphthyl substituent at the C2 position were found to construct S_1 and T_1 states in β-**CQNN** (Fig. S12b, ESI†). A clear difference in the T_2 surface, which is predominantly localized on the naphthyl ring attached to the C4 position of the quinolinyl ring is observed.

Furthermore, calculations shows that the energy levels of the S_1, T_1 and T_2 states of both phases are $^1n\pi^*$, $^3\pi\pi^*$, and $^3\pi\pi^*$ in nature. We have calculated the $\Delta E_{S_1-T_2}$ values in both phases, which are found to be 0.735 eV and 0.016 eV, respectively (Table S6, ESI†). In addition, we found in the calculations that the $\Delta E_{S_1-T_1}$ values, which remain almost the same in both phases, are significantly higher than the $\Delta E_{S_1-T_2}$ values (Table S6, ESI†). This is an indication that a low value of $\Delta E_{S_1-T_2}$ in β-**CQNN** might enable TADF *via* rISC from the T_2 to S_1 state, and RTP from the T_1 state, which is populated *via* either internal conversion (IC) from T_2 or ISC from S_1 states. These observations further substantiate our experimental

results, and set a new example for ML research that involves modulation of triplet states *via* MFICC.

To test the ML properties, we synthesized **CQNP** and **CQPN** (ESI†), in which the C2 and C4 positions of the quinolinyl fragment are alternatively substituted with naphthyl and/or phenyl rings that affect torsions associated with them. Comparison of the SCXRD analysis of **CQNP**, **CQPN**, α-**CQNN** and β-**CQNN** revealed that a significant difference in their torsions associated with the naphthyl and/or phenyl, and carbazolyl rings at the C2, C4, and C8 positions of the quinolinyl moiety was observed. Spectroscopic measurements along with computational analysis show that a TADF *via* rISC from the T_1 to S_1 state is activated in **CQNP** due to its low $\Delta E_{S_1-T_1}$ (0.01 eV) (Fig. S13 and Table S6, ESI†), while the relatively larger $\Delta E_{S_1-T_1}$ (1.67 eV) of **CQPN** resulted in prompt fluorescence features (Table S7, ESI†). It should be noted that no ML properties have been realized in both cases. These observations indicate that sterically crowded **CQNN** can alter its triplet energy level (T_2) *via* MFICC that leads to TADF and RTP under ambient conditions.

In summary, we have synthesized three naphthyl appended carbazole–quinoline conjugates (**CQNN**, **CQNP**, **CQPN**), in which only **CQNN** in solvent-dependent crystallization yielded non-centrosymmetric (α-**CQNN**) and centrosymmetric (β-**CQNN**) phases. Based on photoluminescence spectra and TD-DFT calculations, the centric β-**CQNN** showed both TADF and RTP, while prompt fluorescence and RTP components have been observed in non-centric α-**CQNN**. We have established that mechanical grinding of α-**CQNN** can regenerate the emission of β-**CQNN** *via* modulation of the T_2 energy level caused by mechanical-force induced conformational change. This study, which has led to efficient utilization of both singlet and triplet states for intrinsic dual emission, offers the opportunity to improve our understanding of the mechanical regulation of dual light emitters.

D. R. is grateful to the Science & Engineering Research Board (SERB) (File No: SB/EMEQ-004/2014), DST, the Board of Research and Nuclear Science (BRNS) (File No. 37(3)/14/08-2018-BRNS/37130), DAE, and Shiv Nadar University (SNU) for generous support. I. B. and N. A. thank SNU for fellowships. We thank Mr Anil Kumar for X-ray data collection. We gratefully acknowledge the use of the MAGUS supercomputing system at SNU.

Conflicts of interest

There are no conflicts to declare.

Notes and references

1 (*a*) H. Uoyama, K. Goushi, K. Shizu, H. Nomura and C. Adachi, *Nature*, 2012, **492**, 234; (*b*) Q. Zhang, J. Li, K. Shizu, S. Huang, S. Hirata, H. Miyazaki and C. Adachi, *J. Am. Chem. Soc.*, 2012, **134**, 14706; (*c*) F. B. Dias, T. J. Penfold and A. P. Monkman, *Methods Appl. Fluoresc.*, 2017, **5**, 012001; (*d*) C. Baleizão, S. Nagl, S. M. Borisov, M. Schäferling, O. S. Wolfbeis and M. N. Berberan-Santos, *Chem. – Eur. J.*, 2007, **13**, 3643.

2 (*a*) N. J. Turro, V. Ramamurthy and J. C. Scaiano, *Principles of Molecular Photochemistry*, University Science Books, Sausalito, CA, 2009; (*b*) M. A. El-Sayed, *Acc. Chem. Res.*, 1968, **1**, 8–16; (*c*) O. Bolton, K. Lee, H. J. Kim, K. Y. Lin and J. Kim, *Nat. Chem.*, 2011, **3**, 205; (*d*) S. Hirata, K. Totani, J. Zhang, T. Yamashita, H. Kaji, S. R. Marder, T. Watanabe and C. Adachi, *Adv. Funct. Mater.*, 2013, **23**, 3386; (*e*) D. Lee, O. Bolton, B. C. Kim, J. H. Youk, S. Takayama and J. Kim, *J. Am. Chem. Soc.*, 2013, **135**, 6325.

3 (*a*) C. Adachi, M. A. Baldo, M. E. Thompson and S. R. Forrest, *J. Appl. Phys.*, 2001, **90**, 5048; (*b*) M. A. Baldo, D. F. O'Brien, Y. You, A. Shoustikov, S. Sibley, M. E. Thompson and S. R. Forrest, *Nature*, 1998, **395**, 151.

4 (*a*) I. Bhattacharjee, N. Acharya, S. Karmakar and D. Ray, *J. Phys. Chem. C*, 2018, **122**, 21589; (*b*) D. Lee, O. Bolton, B. C. Kim, J. H. Youk, S. Takayama and J. Kim, *J. Am. Chem. Soc.*, 2013, **135**, 6325.

5 (*a*) H. Bhatia, I. Bhattacharjee and D. Ray, *J. Phys. Chem. Lett.*, 2018, **9**, 3808; (*b*) Z. An, C. Zheng, Y. Tao, R. Chen, H. Shi, T. Chen, Z. Wang, H. Li, R. Deng, X. Liu and W. Huang, *Nat. Mater.*, 2015, **14**, 685.

6 G. Zhang, G. M. Palmer, M. W. Dewhirst and C. L. Fraser, *Nat. Mater.*, 2009, **8**, 747.

7 (*a*) J. Picard, *Science*, 1939, **89**, 460; (*b*) S. J. Toal, K. A. Jones, D. Magde and W. C. Trogler, *J. Am. Chem. Soc.*, 2005, **127**, 11661.

8 (*a*) C. E. Olson, M. J. R. Previte and J. T. Fourkas, *Nat. Mater.*, 2002, **1**, 225; (*b*) M. Irie, T. Fukaminato, T. Sasaki, N. Tamai and T. Kawai, *Nature*, 2002, **420**, 759.

9 A. Kishimura, T. Yamashita, K. Yamaguchi and T. Aida, *Nat. Mater.*, 2005, **4**, 546–549.

10 (*a*) J. Li, C. Nagamani and J. S. Moore, *Acc. Chem. Res.*, 2015, **48**, 2181; (*b*) N. C. Eddingsaas and K. S. Suslick, *Nature*, 2006, **444**, 163; (*c*) N. C. Eddingsaas and K. S. Suslick, *J. Am. Chem. Soc.*, 2007, **129**, 6718; (*d*) J. W. Chung, Y. You, H. S. Huh, B. K. An, S. J. Yoon, S. H. Kim, S. W. Lee and S. Y. Park, *J. Am. Chem. Soc.*, 2009, **131**, 8163–8172.

11 (*a*) Z. Chi, X. Zhang, B. Xu, X. Zhou, C. Ma, Y. Zhang, S. Liua and J. Xu, *Chem. Soc. Rev.*, 2012, **41**, 3878; (*b*) M. Irie, T. Fukaminato, T. Sasaki, N. Tamai and T. Kawai, *Nature*, 2002, **420**, 759–760; (*c*) T. Mutai, H. Satou and K. Araki, *Nat. Mater.*, 2005, **4**, 685–687; (*d*) Y. Sagara and T. Kato, *Nat. Chem.*, 2009, **1**, 605–610.

12 (*a*) J. Kunzelman, M. Kinami, B. R. Crenshaw, J. D. Protasiewicz and C. Weder, *Adv. Mater.*, 2008, **20**, 119–120; (*b*) Y. Sagara and T. Kato, *Angew. Chem., Int. Ed.*, 2008, **47**, 5175–5178; (*c*) X. Luo, J. Li, C. Li, L. Heng, Y. Q. Dong. Zhengping, L. Z. Bo and B. Z. Tang, *Adv. Mater.*, 2011, **23**, 3261–3262.

13 (*a*) Z. Xie, T. Yu, J. Chen, E. Ubba, L. Wang, Z. Mao, T. Su, Y. Zhang, M. P. Aldred and Z. Chi, *Chem. Sci.*, 2018, **9**, 5787; (*b*) H. Wu, C. Hang, X. Li, L. Yin, M. Zhu, J. Zhang, Y. Zhou, H. Ågren, Q. Zhang and L. Zhu, *Chem. Commun.*, 2017, **53**, 2661; (*c*) J. Yang, X. Gao, Z. Xie, Y. Gong, M. Fang, Q. Peng, Z. Chi and Z. Li, *Angew. Chem., Int. Ed.*, 2017, **56**, 15299.

14 (*a*) Z. Mao, Z. Yang, Y. Mu, Y. Zhang, Y.-F. Wang, Z. Chi, C.-C. Lo, S. Liu, A. Lien and J. Xu, *Angew. Chem., Int. Ed.*, 2015, **54**, 1; (*b*) Y. Sagara, S. Yamane, M. Mitani, C. Weder and T. Kato, *Adv. Mater.*, 2016, **28**, 1073; (*c*) J. Yang, Z. Ren, Z. Xie, Y. Liu, C. Wang, Y. Xie, Q. Peng, B. Xu, W. Tian, F. Zhang, Z. Chi, Q. Li and Z. Li, *Angew. Chem., Int. Ed.*, 2016, **55**, 1.

15 I. Bhattacharjee, N. Acharya, H. Bhatia and D. Ray, *J. Phys. Chem. Lett.*, 2018, **9**, 2733.

16 A. D. Becke, *J. Chem. Phys.*, 1993, **98**, 5648.

17 C. Lee, W. Yang and R. G. Parr, *Phys. Rev. B: Condens. Matter Mater. Phys.*, 1988, **37**, 785.

18 E. Runge and E. K. Gross, *Phys. Rev. Lett.*, 1984, **52**, 997.

19 M. J. Frisch, *et al.*, *Gaussian 09 (Revision D.01)*, Gaussian, Inc., Wallingford, CT, 2013.

